



Cite this: *Nanoscale Adv.*, 2023, 5, 6958

## Manipulation of the electrical and memory properties of MoS<sub>2</sub> field-effect transistors by highly charged ion irradiation†

Stephan Sleziona <sup>\*a</sup> Aniello Pelella, <sup>b</sup> Enver Faella, <sup>b</sup> Osamah Kharsah, <sup>a</sup> Lucia Skopinski, <sup>a</sup> André Maas, <sup>a</sup> Yossarian Liebsch, <sup>a</sup> Jennifer Schmeink, <sup>a</sup> Antonio Di Bartolomeo <sup>b</sup> and Marika Schleberger

Field-effect transistors based on molybdenum disulfide (MoS<sub>2</sub>) exhibit a hysteresis in their transfer characteristics, which can be utilized to realize 2D memory devices. This hysteresis has been attributed to charge trapping due to adsorbates, or defects either in the MoS<sub>2</sub> lattice or in the underlying substrate. We fabricated MoS<sub>2</sub> field-effect transistors on SiO<sub>2</sub>/Si substrates, irradiated these devices with Xe<sup>30+</sup> ions at a kinetic energy of 180 keV to deliberately introduce defects and studied the resulting changes of their electrical and hysteretic properties. We find clear influences of the irradiation: while the charge carrier mobility decreases linearly with increasing ion fluence (up to only 20% of its initial value) the conductivity actually increases again after an initial drop of around two orders of magnitude. We also find a significantly reduced n-doping ( $\approx 10^{12} \text{ cm}^{-2}$ ) and a well-developed hysteresis after the irradiation. The hysteresis height increases with increasing ion fluence and enables us to characterize the irradiated MoS<sub>2</sub> field-effect transistor as a memory device with remarkably longer relaxation times ( $\approx$  minutes) compared to previous works.

Received 20th July 2023  
Accepted 24th October 2023

DOI: 10.1039/d3na00543g  
[rsc.li/nanoscale-advances](http://rsc.li/nanoscale-advances)

## 1 Introduction

Molybdenum disulfide (MoS<sub>2</sub>), a member of the family of the so-called transition metal dichalcogenides (TMDCs), is one of the most studied two-dimensional (2D) materials right after graphene. While in its bulk (3D) form it has an indirect bandgap of around 1.2 eV,<sup>1</sup> it develops a direct bandgap of 1.8–1.9 eV (ref. 2) when reduced to its covalently bonded S–Mo–S monolayer structure. This bandgap allows the utilization as typical building blocks for modern electronics like *e.g.*, field-effect transistors (FETs) based on atomically thin 2D materials.<sup>3</sup> Because of that, it was quickly realized that monolayer MoS<sub>2</sub> might be an excellent candidate for future electronic and optoelectronic applications, especially when large scale production techniques such as chemical vapor deposition (CVD) are used. The on-going reduction of device dimensions poses critical problems for traditional semiconductor devices *e.g.* based on silicon, as the carrier mobility degrades rapidly for channel thicknesses reaching the scale of only a few nm,<sup>4–6</sup> which is not the case for MoS<sub>2</sub> and other 2D materials.<sup>7</sup> Indeed it was

demonstrated that MoS<sub>2</sub> FETs with a small gate length ( $\leq 10$  nm) a simultaneously reasonable mobility and high on-currents can be achieved.<sup>8,9</sup> Open challenges for 2D-TMDC FETs to date are Schottky barriers at the metal-TMDC interface,<sup>10,11</sup> non-sufficient doping techniques<sup>12</sup> and structural defects either in the channel material or in the underlying oxide.<sup>13</sup> These structural defects can trap charges and act as scattering centres, modifying the electrical properties of the devices. One prominent consequence of these defects is the occurrence of a hysteresis in the transfer characteristics ( $I_{DS}(V_{GS})$ ) of a FET, which is commonly observed for MoS<sub>2</sub> (and other TMDC) based devices.<sup>14–18</sup> The trapped charges influence the charge carriers in the 2D material channel and shift the transfer characteristics depending on the gate voltage sweep direction. Although most of the time the hysteresis should be prevented or eliminated for stable device performance, it can also be exploited to achieve atomically thin memory devices.<sup>15,19–21</sup>

Defects can be artificially and controllably introduced into 2D materials by particle irradiation, *e.g.* using electrons or ions as projectiles. While electron irradiation often leads to the creation of single vacancies,<sup>22–24</sup> ion irradiation can additionally cause more complex defects, depending on the ion type and energy.<sup>25–28</sup> These defects have been proposed or even utilized for a broad variety of applications, *e.g.* ultrafiltration,<sup>29,30</sup> DNA sequencing<sup>31,32</sup> or catalysis.<sup>33</sup> By fine tuning the energy of the ions, irradiation can even be used to clean the surface of 2D materials from process residues stemming from transfer and

<sup>a</sup>Faculty of Physics and CENIDE, University of Duisburg-Essen, Lotharstraße 1, D-47057 Duisburg, Germany. E-mail: stephan.sleziona@uni-due.de

<sup>b</sup>Department of Physics “E. R. Caianiello”, University of Salerno, and CNR-SPIN, via Giovanni Paolo II, Fisciano, 84084, Salerno, Italy

† Electronic supplementary information (ESI) available. See DOI: <https://doi.org/10.1039/d3na00543g>



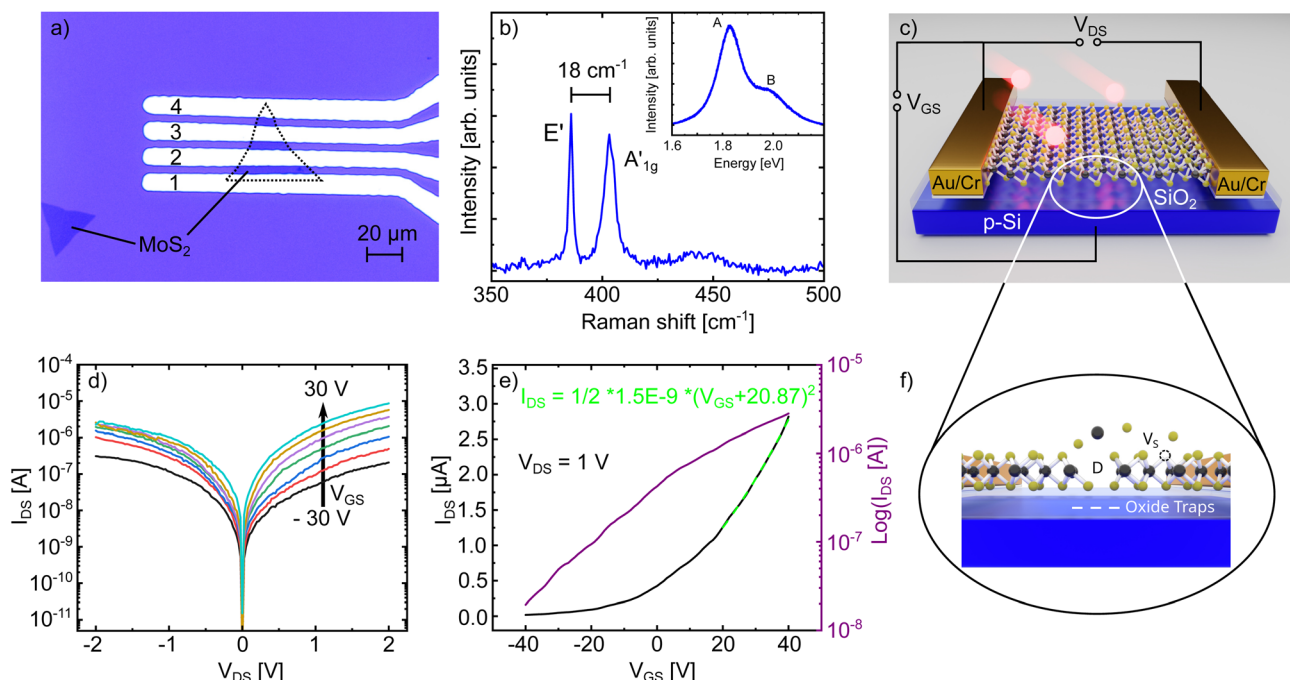


**Fig. 1** (a) Optical microscopy image of monolayer MoS<sub>2</sub> on SiO<sub>2</sub> contacted with four Cr/Au leads. (b) Raman spectrum of monolayer MoS<sub>2</sub> with corresponding photoluminescence spectrum as inset. (c) Schematic of the device and measurement setup used in this work. In (f) we show a schematic representation of the different possible defect types that might be introduced in our devices due to the irradiation. Large and complex defects in the MoS<sub>2</sub> lattice are represented by *D*, while *V<sub>S</sub>* denotes sulphur vacancies. The white lines in the oxide are a schematic representation of electron trap states. (d) Output and (e) transfer characteristics of one of our devices before the irradiation.

lithography steps, without damaging the underlying 2D material too much.<sup>34,35</sup> The irradiation of MoS<sub>2</sub> with electrons or ions with a moderate kinetic energy in the keV range can lead to single or double vacancy defects in the TMDC lattice,<sup>36-38</sup> like *e.g.*, a sulphur vacancy *V<sub>S</sub>* shown schematically in Fig. 1(f). In this work, we use highly charged ions (HCI) with a charge state *q* = 30+ at a kinetic energy *E<sub>kin</sub>* = 180 keV to deliberately introduce defects. We chose HCIs since their potential energy (*i.e.* their charge state) and kinetic energy can be tuned independently and by that control the defect creation in our devices. In contrast to singly charged ions with keV kinetic energy, the defect creation mechanism by HCIs in 2D materials is still under discussion.<sup>24</sup> For free-standing MoS<sub>2</sub>, the formation of nm-sized pores was observed after irradiation with HCIs with the same kinetic energy used in this work. The size of the pores depends on the charge state of the ions<sup>39</sup> and no vacancy-type defects were reported. Since there are, to the best of our knowledge, no corresponding imaging experiments for substrate-supported MoS<sub>2</sub> proving the contrary, it is feasible to assume that the irradiation with HCIs also creates these nm-sized holes in substrate-supported MoS<sub>2</sub>. Recent time-of-flight mass spectrometry experiments show that the kinetic energy of the HCIs has to be taken into account to account for ion-induced damage of substrate supported MoS<sub>2</sub> and that the type of the substrate is important.<sup>40</sup> With the parameters used in this work we thus expect pores in the MoS<sub>2</sub> and a substantial amount of defects in the underlying substrate.

Although there has been done some prior work with particle irradiation of 2D FETs<sup>41-44</sup> these articles focus mostly only on

standard electrical performance like conductivity, mobility, and irradiation hardness<sup>45-47</sup> but not on the hysteretic properties of the irradiated devices. Also, compared to previous studies, where MoS<sub>2</sub> devices were irradiated with singly charged ions (*like e.g.* Ar<sup>+</sup>, N<sup>+</sup>, He<sup>+</sup>),<sup>48-50</sup> in this work, we take a new approach and use HCIs with significantly lower irradiation fluences to realize strong modifications of the devices properties. Furthermore, we pay specific attention to the manipulation of the hysteretic properties of 2D MoS<sub>2</sub> FETs by ion irradiation.

To this end we fabricate CVD-grown single layer MoS<sub>2</sub> FETs on a Si/SiO<sub>2</sub> substrate *via* photolithography and characterize their electrical properties by measuring their output and transfer characteristics. After this initial characterization, the devices are irradiated with HCIs to deliberately introduce defects. We show that the irradiation leads to distinct modifications of the electrical properties and especially causes a strongly reduced n-doping of the devices. Most importantly, we demonstrate that the irradiation leads to the opening of a hysteresis, most likely caused by additional defects in the underlying oxide. The height of the hysteresis scales with the introduced ion fluence, enabling the realisation of a memory device.

## 2 Results and discussion

We begin by describing our devices and the general course of our work. In Fig. 1(a) an optical microscopy image of one of the MoS<sub>2</sub>-FETs used in this work is shown. The four metal contacts, labeled with numbers (1-4). For most devices, we employed

a two-point measurement configuration where two contacts right next to each other were used as drain and source contact. For example, for the device shown in the image, the contacts 1 and 2 were used. Fig. 1(b) shows typical Raman and photoluminescence (PL) data for our FETs after their fabrication. The two well-known  $\text{MoS}_2$  Raman modes  $E'$  and  $A'_{1g}$  are present and the difference in their positions in the spectrum is  $\approx 18 \text{ cm}^{-1}$ . The inset shows the PL spectrum measured at the same spatial position, displaying one strong peak at an energy of 1.83 eV attributed to the A exciton and a smaller peak at an energy of 1.98 eV attributed to the B exciton. Both observations clearly proof that our samples are indeed monolayers of  $\text{MoS}_2$ .<sup>2,51</sup> Fig. 1(c) outlines the general course of our experiment: the FET structure is used for standard electrical characterization of the  $\text{MoS}_2$ , in particular the output ( $I_{\text{DS}}(V_{\text{DS}})$ ) and transfer ( $I_{\text{DS}}(V_{\text{GS}})$ ) characteristics. After this initial characterization, the devices are irradiated with  $\text{Xe}^{30+}$  ions at a kinetic energy of 180 keV to deliberately introduce defects into the devices. Afterwards, the devices are again characterized to observe the influence of the introduced defects on their electrical behavior. We irradiated four different devices with four different fluences, namely 100 ions/ $\mu\text{m}^2$ , 200 ions/ $\mu\text{m}^2$ , 400 ions/ $\mu\text{m}^2$  and 1600 ions/ $\mu\text{m}^2$ .

The output and transfer characteristics of one of our device before the irradiation is shown exemplary in Fig. 1(d) and (e), respectively. The output characteristics displays a slightly rectifying Schottky barrier between the channel and the contacts, which is a common observation for  $\text{MoS}_2$ -FETs, since mid-gap Fermi level pinning arises from defects at various metal-TMDC interfaces caused *e.g.* by the processing conditions.<sup>52-57</sup> The transfer characteristics in Fig. 1(e) reveals the behavior of a normally-on n-type transistor with very strong n-doping.  $\text{MoS}_2$  is typically found to be n-doped, which is attributed to electron-donating sulfur vacancies.<sup>58-61</sup> Consequently, the off-state of the transistor can not be reached in the applied gate voltage range, so the ratio between the minimum and maximum current is only  $10^3$ . We note that the devices in this work exhibit small differences in their overall electrical behavior, which is a typical observation for 2D devices in literature and can be explained by the contact resistance and Fermi-level pinning being delicately dependent on microscopic details in the contact formation at the metal-TMDC interface.<sup>55,62</sup> Nevertheless, all our devices have in common that they have a low Schottky barrier and exhibit strong n-doping.

In Fig. 2(a) and (b) the output and transfer characteristics of the  $\text{MoS}_2$  device before (blue) and after irradiation (red) with a fluence of 400 ions/ $\mu\text{m}^2$  are shown. Let us discuss the output characteristic in Fig. 2(a) first. It displays a reduction of the current by around two orders of magnitude after the irradiation. Besides that, the Schottky type behavior is not modified. This finding is within our expectations: particle irradiation of contacts can modify the metal-2D material interface in such devices and lead to reduced contact resistance and Schottky barriers.<sup>63,64</sup> In our work however, the kinetic energy of the ions is not high enough to penetrate through the metal contacts, as supported by SRIM calculations that demonstrate that all ion collision events occur only in the metal and not at the interface (see Fig. S1a†). This means that all the energy of the ions is

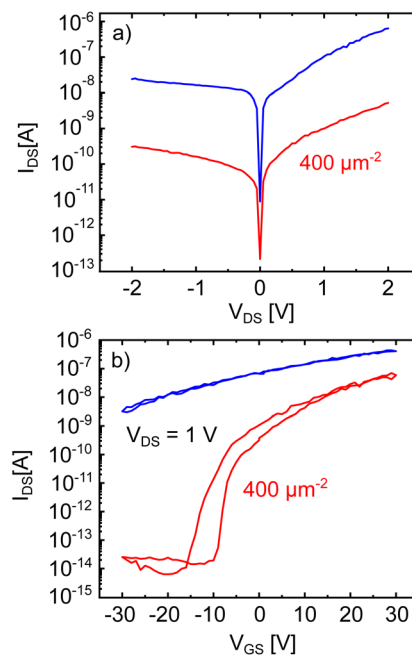


Fig. 2 (a) Output and (b) transfer characteristics of a  $\text{MoS}_2$  FET before (blue) and after (red) irradiation with  $\text{Xe}^{30+}$  ions with a fluence of 400 ions/ $\mu\text{m}^2$ .

deposited into the metal and not at the metal-TMDC interface, from which follows, that the interface can not be modified by the irradiation.

The strong reduction of  $I_{\text{DS}}$  indicates a significant increase in scattering centers. Regardless of the specific defect type created by the irradiation (vacancies, holes, strained/chemically modified lattice), all of them will pose scattering centres for the charge carriers and thus reduce the conductivity of our device. We will now discuss the transfer characteristics in Fig. 2(b) which shows striking differences between the measurement before (blue) and after (red) the irradiation. As discussed for Fig. 1(e), the transfer characteristics before the irradiation displays a strong n-doping behavior. When sweeping the gate voltage between  $-30 \text{ V}$  and  $+30 \text{ V}$  and back, no hysteresis effect is observed. This might be caused by the strong n-doping of our devices, since the saturation region of the transfer characteristics usually does not show a significant hysteretic behavior when measured in high vacuum conditions.<sup>14,16,21</sup> After the irradiation, the most striking difference is the appearance of the off-state region and a hysteresis in the transfer characteristics. As mentioned before, this hysteresis is generally attributed to either defects in the  $\text{MoS}_2$  lattice, at the  $\text{MoS}_2$ /oxide interface or in the oxide itself.<sup>16,21,65</sup> As the occurrence of the hysteresis is clearly related to the irradiation it seems straightforward to claim that it is a result of additional defects introduced by the irradiation. The right-shift of the transfer after the forward gate voltage sweep, which leads to the clockwise hysteresis, is indicative of negative charge trapping. A further discussion of the properties of the hysteresis and which type of defect is likely the reason for its occurrence will be conducted later on. Additionally, the transfer curve shows, that the n-doping of the



device is strongly reduced after the irradiation, since the threshold voltage ( $V_{th}$ ) shifts towards positive gate voltages. It is now even possible to reach the off-state of the transistor in the applied gate voltage range and a high on-off ratio of nearly 6 orders of magnitude can be derived.

This reduction of n-type doping may be attributed to several possible causes. Oxygen molecules capture electrons in  $\text{MoS}_2$  (ref. 66–68) and at the dangling bonds of the 2D material defect sites the chemical and physical adsorption of molecules can be enhanced.<sup>69–71</sup> Although the amount of adsorbed molecules should be reduced under vacuum conditions, ion irradiation can lead to the formation of chemically adsorbed  $\text{MoO}_3$  at the defect edges, which would be very resistant to vacuum assisted desorption<sup>33</sup> and could also explain the observed reduction in n-doping. Since the HCIs will not only deposit their energy in the  $\text{MoS}_2$  monolayer, but also in the underlying  $\text{SiO}_2$  substrate, defects in the oxide could also play a role in p-doping the device. In fact, electron-trapping defect states for  $\text{MoS}_2$  on a  $\text{SiO}_2$  substrate have already been reported<sup>65,72,73</sup> and would lead to an effective p-doping of our devices by an additional gating effect (see schematic representation of oxide traps in Fig. 1(f)). The trapped negative charges in the oxide influence the electric field generated by the applied gate voltage and thereby shifting the transfer curve towards positive gate voltages.

In the following, we will compare the results of the electrical characterization before and after the irradiation of our devices in dependence of the irradiation fluence. For this, we will address the conductivity, mobility, and charge carrier density, starting with the conductivity. In Fig. 3(a) we display the remaining conductivity ( $\sigma/\sigma_0$ ) using the output characteristics

before and after irradiation. That is, we normalized the conductivity after irradiation to its value before irradiation to compare the different devices with each other. Interestingly, the devices show an increasing remaining conductivity with increasing ion fluence, after the initial drop in conductivity already discussed above (see Fig. 2(a)). This unintuitive increase of electrical conductivity with increasing ion fluence was first reported by Fox *et al.*<sup>74</sup> for the irradiation of bilayer  $\text{MoS}_2$  with He-ions. This peculiar behavior could be connected to an irradiation induced activation of an additional transport mechanism. For 2D TMDCs it has already been shown, that an increase in chalcogen vacancies or interface defects can lead to hopping transport *via* localized states and, as a consequence, lead to an increasing conductivity.<sup>58,75</sup> Nevertheless, temperature-dependent conductivity measurements would be needed to confirm a change in the transport mechanism due to the irradiation.<sup>76,77</sup>

Note, that the FET irradiated with  $200 \text{ ions}/\mu\text{m}^2$  is the only exception to the otherwise linear behavior. For this device we used the contacts 1 and 3 as source and drain contact with one contact (2) in between on the  $\text{MoS}_2$  channel (see Fig. 1(a)). By Fermi-level pinning this contact can modify the electrical behavior of the 2D material channel, which is mirrored in all electrical characterizations (Fig. 3(a)–(c)). We have therefore excluded this data point from our discussion.

Next, we calculate the effective mobility by fitting the equation  $I_{DS} = \frac{W}{L} \mu_{eff} Q_n V_{DS}$  to the transfer characteristics at high gate voltages ( $> 20 \text{ V}$ ). With  $Q_n = C_{ox}(V_{GS} - V_{th})$  and  $C_{ox} = 1.21 \times 10^{-8} \text{ F cm}^{-2}$  we obtain values between  $0.5\text{--}10 \text{ cm}^2 \text{ V}^{-1} \text{ s}^{-1}$  for

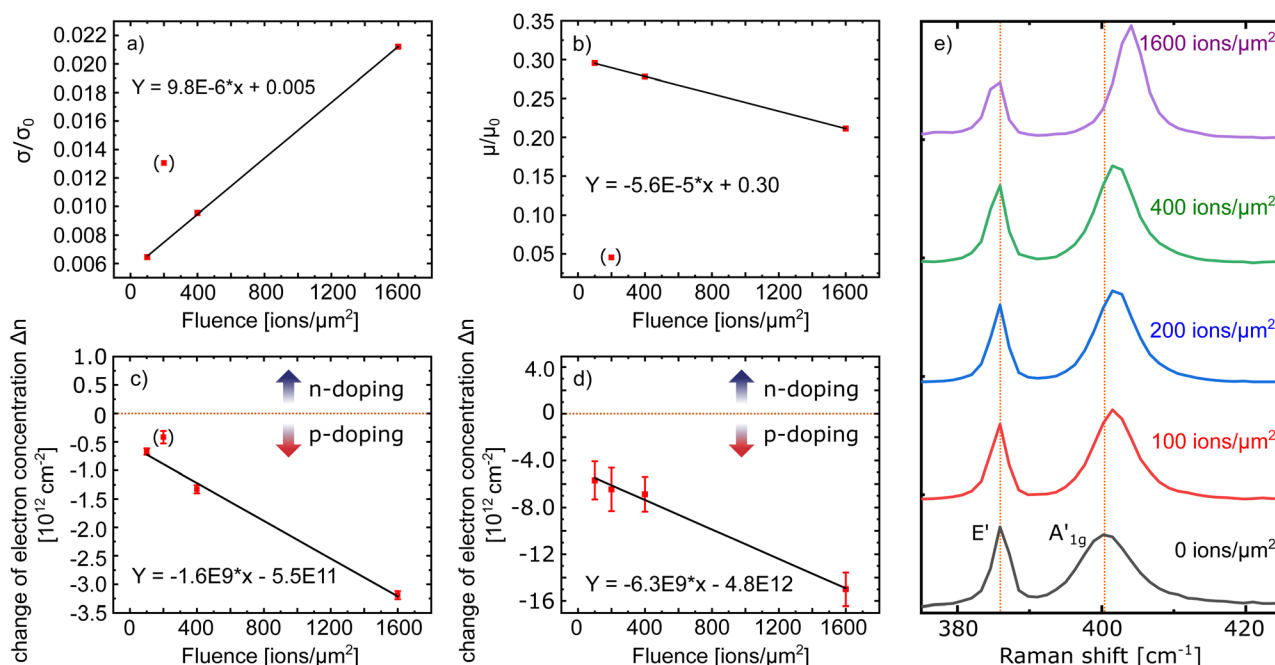


Fig. 3 (a) Remaining conductivity of the  $\text{MoS}_2$  FETs after the irradiation with different fluences normalized to the respective value of the device before the irradiation ( $\sigma/\sigma_0$ ). (b) Effective mobility of the  $\text{MoS}_2$  FETs after the irradiation with different fluences normalized to the respective value of the device before the irradiation ( $\mu/\mu_0$ ). (c) Change in charge carrier concentration of the  $\text{MoS}_2$  FETs for the different fluences calculated by the shift of  $V_{th}$ . Negative values indicate a decrease of the electron density, meaning increased p-doping. (d) Change in charge carrier concentration for the different fluences calculated from the Raman spectra in (e) which are taken from a  $\text{MoS}_2$  sample at the different irradiation fluences.



the devices used in this work, which is in the range typically measured for such devices.<sup>14,78,79</sup> After the irradiation, the mobility was examined again and then normalized to the value measured before the irradiation ( $\mu/\mu_0$ ). The results of this analysis are shown in Fig. 3(b) displaying a monotonous decrease of the mobility with increasing ion fluence. The defects introduced by the HCl irradiation either in the MoS<sub>2</sub> or in the oxide can lead to increased Coulomb scattering for the charge carriers in our devices by charge trapping. This leads to shorter scattering times and therefore an overall reduced mobility, despite the enhanced remaining conductivity.

While nm-sized holes created in the MoS<sub>2</sub> lattice by HCl irradiation would certainly act as scattering centres for the charge carriers in the device, the SRIM calculations in Fig. S1b† demonstrate, that for a MoS<sub>2</sub> monolayer on top of a SiO<sub>2</sub> substrate, most of the collisions happen in the SiO<sub>2</sub> when this system is irradiated with Xe<sup>+</sup> ions at a kinetic energy of 180 keV. Around 90% of the collisions within the first few nm happen in the oxide, pointing towards oxide defects playing the dominant role for the reduction of the mobility due to the irradiation.

Lastly, we discuss the change in charge carrier density. We quantitatively evaluate the change in doping for our devices using the transfer characteristics of each device before and after irradiation. Because of the initially high n-doping of our devices we use  $I_{DS} = \mu_v C_{ox} \frac{W}{L} (V_{GS} - V_{th})^2 V_{DS}$  to fit the transfer curve and extract the value for  $V_{th}$  (see green-streaked line in Fig. 1(e)).<sup>16</sup> From this we calculated the change in charge carrier concentration with  $\Delta n = C_{ox} \times \frac{\Delta V_{th}}{q}$ . As can be seen in Fig. 3(c), the irradiation leads to less n-doping (*i.e.* effective p-doping) in our devices in the order of  $10^{12} \text{ cm}^{-2}$  and increases with increasing ion fluence up to  $3.0 \times 10^{12} \text{ cm}^{-2}$  without any indication of a saturation behavior.

To further confirm this finding, we performed Raman spectroscopy of a CVD-grown MoS<sub>2</sub> sample between the different irradiation steps (see Fig. 3(e)). The qualitative behavior of the Raman spectra, a constant position for the E' mode, while the A'₁g mode shifts to higher wavenumbers, points to decreasing n-doping,<sup>80</sup> as it was also derived from the transfer characteristics. We also find a stronger reduction of the n-doping with increasing ion fluence. For a quantitative analysis we used the procedure from ref. 81. The result of this is shown in Fig. 3(d). Obviously, both methods, electrical characterization and evaluation of Raman spectra, yield the same result, a linearly decreasing n-doping with increasing irradiation fluence, supporting our previous findings.

Possible mechanisms for a decrease of n-doping, like the adsorption of oxygen molecules at defect sites or electron capturing defects in the oxide, were already discussed above. With increasing ion fluence, the density of these defects increases and we therefore infer, that the irradiation does create electron capturing defects. This is also confirmed by the fact, that the absolute values extracted from the FET transfer characteristics are somewhat lower than those extracted from the Raman data, as the FETs were measured under high vacuum conditions (defects in the MoS<sub>2</sub> are not saturated by oxygen and

thus do not contribute to the reduction), while the Raman spectra were collected in ambient conditions (both types of defects contribute).

We note, that the change in charge carrier density as derived by both methods is  $\approx 10^{12}\text{--}10^{13} \text{ cm}^{-2}$  and thus 1–2 orders of magnitude higher than the irradiation fluence. As already discussed above, defect sites will facilitate p-doping. The defects we induce here are not point-like, but have a spatial extension on the order of nm. We therefore expect a high number of dangling bonds at the defect edges, which are prone to the adsorption or even bonding of gas molecules, explaining the high efficiency in terms of p-doping per ion. For the other possible cause of the observed doping effect, electron trapping defects in the SiO<sub>2</sub> substrate, there will also several defects per ion be created (see discussion below). This is also consistent with the high efficiency in terms of doping per ion. Therefore, the observed doping effect can be explained satisfactorily by both possibilities: either defects in the MoS<sub>2</sub> channel or in the underlying oxide. Since the measurements were performed under high vacuum conditions, defects in the oxide seem more likely.

Finally, we want to address the manipulation of the hysteresis' properties of the MoS<sub>2</sub> devices by ion irradiation. As it was already shown in Fig. 2(b) after the irradiation, a hysteresis can be observed in the devices transfer characteristics, which was absent before the irradiation. The origin of the hysteresis is generally attributed to defects, either in the MoS<sub>2</sub> channel, the MoS<sub>2</sub>/oxide interface or in the oxide itself.<sup>14,65,82–84</sup> From an application point of view, such a device may be used as a non-volatile storage element. Favorable properties are two stable and clearly distinguishable memory states, the so-called memory window, a sufficiently high hysteresis to prevent unwanted switching and long time-constants when switched by erase/write voltage pulses.

For our analysis, we first evaluate the memory window, *i.e.*, the height of the hysteresis (*i.e.*  $\Delta I_{DS}$  at the same  $V_{GS}$ ) for the different irradiation fluences. The results found for our different devices are summarized in Fig. 4(a). The hysteresis' height increases linearly with increasing ion fluence reaching up to around two orders of magnitude for the device irradiated with the highest fluence. We note, that even for the smallest irradiation fluence of only  $100 \text{ ions}/\mu\text{m}^2$  there is already a fully developed hysteresis observable even though it was nearly absent prior to the irradiation (see Fig. S2†). These results clearly demonstrate, that ion induced defects are responsible for the observed hysteresis.

To study the switching behavior of our device we applied  $\pm 30 \text{ V}$  gate pulses and recorded the transient behavior of the device irradiated with a fluence of  $200 \text{ ions}/\mu\text{m}^2$ . The result is shown in Fig. 4(b). In this device we can reach two distinct memory states at a gate voltage of  $V_{GS} = 0 \text{ V}$  with a current separation of around one order of magnitude. The current separation prevails and is stable for the entire observed pulse interval (around 30 min), which is comparable with the retention times observed in few-layer MoS<sub>2</sub> charge-trapping memory devices.<sup>85,86</sup> The transients observed in Fig. 4(b) can be interpreted in terms of charge trapping/detrapping

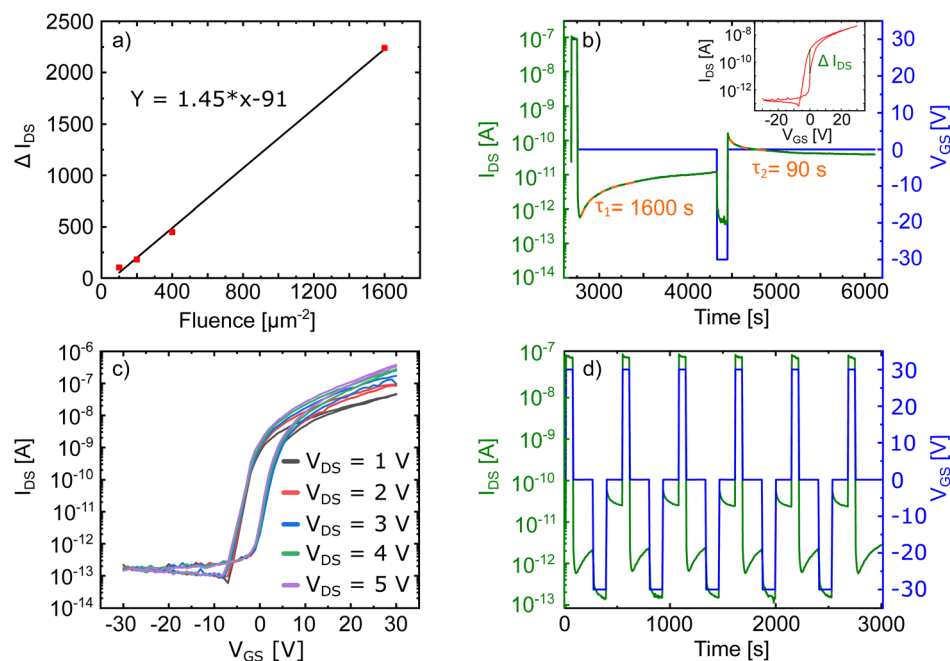


Fig. 4 (a) Hysteresis height (maximum  $\Delta I_{DS}$  at the same  $V_{GS}$ , see also inset in (b)) evaluated from the transfer characteristics of each device after the irradiation with different fluences. (b) Transient behavior of the device irradiated with a fluence of  $200 \text{ ions}/\mu\text{m}^2$  for a single set–read–reset–read cycle. The dashed orange curves correspond to fits of exponential decays from which the trapping times  $\tau_1$  and  $\tau_2$  are evaluated. Inset shows the corresponding hysteresis curve with  $\Delta I_{DS}$  highlighted. (c) Transfer characteristics of the device from (b) for different values of  $V_{DS}$ . (d) Several set–read–reset–read cycles of the same device used in (b).

mechanisms. The time constants have been evaluated for the read ( $\tau_1$ ) and the erase ( $\tau_2$ ) configuration by fitting an exponential function  $f(t) = c \times e^{-\frac{t}{\tau}} + A_0$  to the data.

Compared to previous studies, the time constants  $\tau_1 = 1600 \text{ s}$  and  $\tau_2 = 90 \text{ s}$ , respectively, are rather long.<sup>15</sup> This finding points towards oxide defects playing a major role because charges trapped in deep oxide defects have considerably longer relaxation times than *e.g.* traps in the 2D material itself or at the 2D material/oxide interface.<sup>21,87,88</sup> The time constant for the positive gate pulse ( $\tau_1$ ) is much longer than the time constant for negative gate pulse ( $\tau_2$ ). This is also another indicator of negatively charged oxide defects being the main contribution to the hysteresis in our work. These defects lie in the vicinity of the conduction band of  $\text{MoS}_2$  (ref. 65) and would therefore be charged when applying positive gate voltages, but would not be charged for the negative gate pulse. Additionally, we show in Fig. 4(c) that the observed hysteresis is independent of the applied  $V_{DS}$  within the range of  $1 \text{ V}$ – $5 \text{ V}$ . This is in contrast to recent observations for black phosphorous FETs, where the dependence of the hysteresis on  $V_{DS}$  was ascribed to defects in the 2D material channel itself.<sup>89</sup> Considering our irradiation conditions, significant defect generation in the substrate is to be expected.

As already discussed above, the SRIM calculations in Fig. S1(b)† demonstrate, that most of the collisions caused by the ion irradiation at this kinetic energy occur in the oxide, since the  $\text{MoS}_2$  channel is atomically thin. We therefore conclude, that while the doping effect may be due to both, ion-induced defects in the  $\text{MoS}_2$  and the substrate, the hysteresis observed in our devices is caused by negatively charged defects

in the underlying oxide induced by the HCI irradiation. With Fig. 4(d) we prove that the separation of the two memory states is stable for several memory cycles.

### 3 Conclusion

We have investigated the manipulation of the electrical properties of  $\text{MoS}_2$  FETs by the irradiation with HCIs. While we found a decreasing mobility in the devices with increasing ion fluence, the conductivity after an initial drop actually increases with higher defect density suggesting that at hopping-like transport takes over with increasing defect density. This further proves, that the devices are rather resistant to ion irradiation, an important factor for the possible use in high radiation environments like *e.g.* space applications.

Additionally, we have shown that HCI irradiation can be used for deliberate and controlled manipulation of the doping density of  $\text{MoS}_2$  devices. In our case we found a strong decrease in n-doping. Most notably, the irradiation leads to a hysteresis in the transfer characteristics of the device which we successfully exploited for a non-volatile memory device with two stable memory states and a long retention time. We demonstrated that the memory window can be tuned by the irradiation fluence, opening up new possibilities to boost the performance of  $\text{MoS}_2$  based memory devices. We also believe, that this procedure can be applied to other similar 2D devices since the hysteresis most likely originates from defects induced into the underlying oxide.

Since the strong modifications of the devices' properties already happen at comparatively low fluences, we observe no notable damage to the active channel and the surrounding



substrate in atomic force microscopy (AFM) images after the irradiation (see Fig. S3†). In particular, we find no evidence of hydrocarbon deposition, which would hinder further processing steps of the devices after the irradiation. This is a big advantage to previous works, where  $\text{MoS}_2$  FETs have been irradiated with He-ions.<sup>49,50</sup>

Further, we like to point out that Chen *et al.*<sup>48</sup> succeeded in realizing a  $\text{MoS}_2$  based non-volatile memory device by seeding defects in the oxide *via* irradiation with  $\text{Ar}^+$  and  $\text{N}^+$  ions before the  $\text{MoS}_2$  was deposited on the substrate, while here, we were able to realize a memory device by irradiating the  $\text{MoS}_2$  after device fabrication. Our approach thus opens up the possibility to fine-tune the electrical and memory properties of devices by choosing the appropriate ion fluence. This, together with the independent control of potential and kinetic energy, will allow to precisely manipulate the electrical properties of the irradiated devices in future experiments.

## 4 Experimental procedure

$\text{MoS}_2$  flakes were grown *via* chemical vapor deposition (CVD) on a highly doped p-type Si substrate (resistivity 0.001–0.005  $\Omega$  cm) covered by 285 nm thermal  $\text{SiO}_2$ . At first a 1% sodium cholate solution was spin coated onto the substrate working as a seeding promoter. The growth was performed in a three-zone (ThermConcept ROK 70/750/12-3z) tube furnace. By 10 min purging with 500 sccm Ar gas (99.9%) flow, the  $\text{O}_2$  content of the furnace was minimized. 40 mg of S powder (99.98% Sigma Aldrich) were placed in the upstream heating zone at 150 °C.  $\text{MoO}_3$ , used as the source for molybdenum, was obtained from a aqueous ammonium heptamolybdate (AHM) solution (ratio 1 : 1) initially annealed at 300 °C for 24 min under ambient conditions and positioned in the next downstream zone at 750 °C. During the whole process 500 sccm of Ar gas flows through the quartz tube. The growth process lasted 30 min and was followed by a rapid cooling. At a temperature of around 100 °C the samples were retrieved from the CVD furnace. The resulting  $\text{MoS}_2$  flakes are mostly single layers with triangular shape.

For device fabrication the freshly grown samples were investigated *via* optical microscopy to select suitable flakes for photolithography processing. After the standard photolithography process 10 nm of Cr and 100 nm of Au were deposited by electron-beam (Cr) and thermal evaporation (Au) at a process pressure of  $1 \times 10^{-5}$  mbar to electrically contact the  $\text{MoS}_2$  flakes.

Electrical characterization of the devices was performed with a cryogenic probe station with pressure control and four metallic nanoprobes, which are connected to a Keithley 4200 SCS. The metallic sample plate was used to apply the backgate voltage to the Si substrate. All electrical measurements in this work are performed under a vacuum of  $1 \times 10^{-4}$  mbar and the samples were left there for at least 12 hours before starting the measurements.

To irradiate the samples, highly charged xenon ions were generated in an electron beam ion source (EBIS) commercially available from Dreebit GmbH, Germany.<sup>90</sup> A kinetic energy of 180 keV (1.4 keV amu<sup>-1</sup>) and an ion charge state of 30+ with a potential energy of 15.4 keV (0.1 keV amu<sup>-1</sup>) was selected *via*

a sector magnet and used for all experiments. Ion irradiation was performed under ultra-high vacuum conditions (pressure about  $4 \times 10^{-9}$  mbar), and each sample was irradiated with a total fluence between 100 and 1600 ions/ $\mu\text{m}^2$ . During the irradiation, the entire devices, including their electrical contacts, are impacted by ions due to the spatial extent (around 1 mm<sup>2</sup>) of the ion beam.

## Author contributions

St. S., M. S. and A. d. B. are responsible for the conceptualization of the project and the experiments. St. S., A. P. and E. F. performed the investigation. St. S. analyzed and evaluated the data. L. S. performed the irradiation and helped with data interpretation. O. K., A. M. and Y. L. fabricated the devices. J. S. performed parts of the investigation and contributed to interpretation and visualization of the data. M. S. and A. d. B. were responsible for funding acquisition and provided resources. St. S was responsible for writing the original draft. All authors contributed to the writing by reviewing and editing the manuscript.

## Conflicts of interest

There are no conflicts to declare.

## Acknowledgements

This work was funded by the Deutsche Forschungsgemeinschaft (DFG, German Research Foundation) – project numbers INST-272132938, INST-429784087, 278162697 (SFB 1242 “Non-equilibrium dynamics in the time domain”), 461605777 (IRTG 2803 2D MATURE) and the Bundesministerium für Bildung und Forschung (BMBF, project number 05K16PG1). We acknowledge support by the clean room staff of A. Lorke, especially G. Prinz. We acknowledge support by the Open Access Publication Fund of the University of Duisburg-Essen. We thank Andreas Reichert for his help with the table of contents.

## Notes and references

- 1 K. K. Kam and B. A. Parkinson, *J. Phys. Chem.*, 1982, **86**, 463–467.
- 2 K. F. Mak, C. Lee, J. Hone, J. Shan and T. F. Heinz, *Phys. Rev. Lett.*, 2010, **105**, 136805.
- 3 B. Radisavljevic, A. Radenovic, J. Brivio, V. Giacometti and A. Kis, *Nat. Nanotechnol.*, 2011, **6**, 147–150.
- 4 K. Uchida, H. Watanabe, A. Kinoshita, J. Koga, T. Numata and S. Takagi, *Digest. International Electron Devices Meeting*, 2002.
- 5 L. Gomez, I. Berg and J. L. Hoyt, *IEEE Electron Device Lett.*, 2007, **28**, 285–287.
- 6 M. Schmidt, M. C. Lemme, H. Gottlob, F. Driussi, L. Selmi and H. Kurz, *Solid-State Electron.*, 2009, **53**, 1246–1251.
- 7 C. D. English, G. Shine, V. E. Dorgan, K. C. Saraswat and E. Pop, *Nano Lett.*, 2016, **16**, 3824–3830.



8 C. D. English, K. K. H. Smithe, R. L. Xu and E. Pop, *2016 International Electron Devices Meeting*, Piscataway, NJ, 2016, pp. 5.6.1–5.6.4.

9 S. B. Desai, S. R. Madhvapathy, A. B. Sachid, J. P. Llinas, Q. Wang, G. H. Ahn, G. Pitner, M. J. Kim, J. Bokor, C. Hu, H.-S. P. Wong and A. Javey, *Science*, 2016, **354**, 99–102.

10 D. S. Schulman, A. J. Arnold and S. Das, *Chem. Soc. Rev.*, 2018, **47**, 3037–3058.

11 A. Grillo and A. Di Bartolomeo, *Adv. Electron. Mater.*, 2021, **7**, 2000979.

12 Q. He, Y. Liu, C. Tan, W. Zhai, G.-H. Nam and H. Zhang, *ACS Nano*, 2019, **13**, 12294–12300.

13 T. Knobloch, S. Selberherr and T. Grasser, *Nanomaterials*, 2022, **12**, 3548.

14 D. J. Late, B. Liu, H. S. S. R. Matte, V. P. Dravid and C. N. R. Rao, *ACS Nano*, 2012, **6**, 5635–5641.

15 F. Urban, F. Giubileo, A. Grillo, L. Iemmo, G. Luongo, M. Passacantando, T. Foller, L. Madauß, E. Pollmann, M. P. Geller, D. Oing, M. Schleberger and A. Di Bartolomeo, *2D Mater.*, 2019, **6**, 045049.

16 A. Di Bartolomeo, L. Genovese, F. Giubileo, L. Iemmo, G. Luongo, T. Foller and M. Schleberger, *2D Mater.*, 2018, **5**, 015014.

17 J. Shu, G. Wu, Y. Guo, B. Liu, X. Wei and Q. Chen, *Nanoscale*, 2016, **8**, 3049–3056.

18 E. Faella, K. Intonti, L. Viscardi, F. Giubileo, A. Kumar, H. T. Lam, K. Anastasiou, M. F. Craciun, S. Russo and A. Di Bartolomeo, *Nanomaterials*, 2022, **12**, 1886.

19 S. Bertolazzi, D. Krasnozhon and A. Kis, *ACS Nano*, 2013, **7**, 3246–3252.

20 G. He, H. Ramamoorthy, C.-P. Kwan, Y.-H. Lee, J. Nathawat, R. Somphonsane, M. Matsunaga, A. Higuchi, T. Yamanaka, N. Aoki, Y. Gong, X. Zhang, R. Vajtai, P. M. Ajayan and J. P. Bird, *Nano Lett.*, 2016, **16**, 6445–6451.

21 N. Kaushik, D. M. A. Mackenzie, K. Thakar, N. Goyal, B. Mukherjee, P. Boggild, D. H. Petersen and S. Lodha, *npj 2D Mater. Appl.*, 2017, **1**, 34.

22 C. Jin, F. Lin, K. Suenaga and S. Iijima, *Phys. Rev. Lett.*, 2009, **102**, 195505.

23 H.-P. Komsa, S. Kurasch, O. Lehtinen, U. Kaiser and A. V. Krasheninnikov, *Phys. Rev. B: Condens. Matter Mater. Phys.*, 2013, **88**, 035301.

24 M. Schleberger and J. Kotakoski, *Materials*, 2018, **11**, 1885.

25 Z. Li and F. Chen, *Appl. Phys. Rev.*, 2017, **4**, 011103.

26 L. Madauß, O. Ochedowski, H. Lebius, B. Ban-d'Etat, C. H. Naylor, A. T. C. Johnson, J. Kotakoski and M. Schleberger, *2D Mater.*, 2017, **4**, 015034.

27 O. Ochedowski, H. Bukowska, V. M. Freire Soler, L. Brökers, B. Ban-d'Etat, H. Lebius and M. Schleberger, *Nucl. Instrum. Methods Phys. Res., Sect. B*, 2014, **340**, 39–43.

28 J. Kotakoski, C. Brand, Y. Lilach, O. Cheshnovsky, C. Mangler, M. Arndt and J. C. Meyer, *Nano Lett.*, 2015, **15**, 5944–5949.

29 D. Cohen-Tanugi and J. C. Grossman, *Nano Lett.*, 2012, **12**, 3602–3608.

30 L. Madauß, J. Schumacher, M. Ghosh, O. Ochedowski, J. Meyer, H. Lebius, B. Ban-d'Etat, M. E. Toimil-Molares, C. Trautmann, R. G. H. Lammertink, M. Ulbricht and M. Schleberger, *Nanoscale*, 2017, **9**, 10487–10493.

31 H. W. C. Postma, *Nano Lett.*, 2010, **10**, 420–425.

32 R. Kozubek, P. Ernst, C. Herbig, T. Michely and M. Schleberger, *ACS Appl. Nano Mater.*, 2018, **1**, 3765–3773.

33 L. Madauß, I. Zegkinoglou, H. Vázquez Muñoz, Y.-W. Choi, S. Kunze, M.-Q. Zhao, C. H. Naylor, P. Ernst, E. Pollmann, O. Ochedowski, H. Lebius, A. Benyagoub, B. Ban-d'Etat, A. T. C. Johnson, F. Djurabekova, B. Roldan Cuenya and M. Schleberger, *Nanoscale*, 2018, **10**, 22908–22916.

34 B. Brennan, A. Centeno, A. Zurutuza, P. Mack, K. R. Paton and A. J. Pollard, *ACS Appl. Nano Mater.*, 2021, **4**, 5187–5197.

35 S. Sleziona, S. Rauls, T. Heckhoff, L. Christen, E. Pollmann, L. Madauß, S. Franzka, A. Lorke, H. Wende and M. Schleberger, *Nanotechnology*, 2021, **32**, 205702.

36 O. Lehtinen, J. Kotakoski, A. V. Krasheninnikov and J. Keinonen, *Nanotechnology*, 2011, **22**, 175306.

37 O. Lehtinen, J. Kotakoski, A. V. Krasheninnikov, A. Tolvanen, K. Nordlund and J. Keinonen, *Phys. Rev. B: Condens. Matter Mater. Phys.*, 2010, **81**, 153401.

38 W. Zhou, X. Zou, S. Najmaei, Z. Liu, Y. Shi, J. Kong, J. Lou, P. M. Ajayan, B. I. Yakobson and J.-C. Idrobo, *Nano Lett.*, 2013, **13**, 2615–2622.

39 R. Kozubek, M. Tripathi, M. Ghorbani-Asl, S. Kretschmer, L. Madauß, E. Pollmann, M. O'Brien, N. McEvoy, U. Ludacka, T. Susi, G. S. Duesberg, R. A. Wilhelm, A. V. Krasheninnikov, J. Kotakoski and M. Schleberger, *J. Phys. Chem. Lett.*, 2019, **10**, 904–910.

40 L. Skopinski, S. Kretschmer, P. Ernst, M. Herder, L. Madauß, L. Breuer, A. V. Krasheninnikov and M. Schleberger, *Phys. Rev. B*, 2023, **107**, 044003.

41 M. G. Stanford, P. R. Pudasaini, A. Belianinov, N. Cross, J. H. Noh, M. R. Koehler, D. G. Mandrus, G. Duscher, A. J. Rondinone, I. N. Ivanov, T. Z. Ward and P. D. Rack, *Sci. Rep.*, 2016, **6**, 27276.

42 E. Zion, A. Haran, A. Butenko, L. Wolfson, Y. Kaganovskii, T. Havdala, A. Sharoni, D. Naveh, V. Richter, M. Kaveh, E. Kogan and I. Shlimak, *Graphene*, 2015, **04**, 45–53.

43 H. Li, C. Liu, Y. Zhang, C. Qi, Y. Wei, J. Zhou, T. Wang, G. Ma, H.-S. Tsai, S. Dong and M. Huo, *Nanotechnology*, 2019, **30**, 485201.

44 S. Bertolazzi, S. Bonacchi, G. Nan, A. Pershin, D. Beljonne and P. Samori, *Adv. Mater.*, 2017, **29**, 1606760.

45 P. Ernst, R. Kozubek, L. Madauß, J. Sonntag, A. Lorke and M. Schleberger, *Nucl. Instrum. Methods Phys. Res., Sect. B*, 2016, **382**, 71–75.

46 S. Kumar, A. Kumar, A. Tripathi, C. Tyagi and D. K. Avasthi, *J. Appl. Phys.*, 2018, **123**, 161533.

47 O. Ochedowski, K. Marinov, G. Wilbs, G. Keller, N. Scheuschner, D. Severin, M. Bender, J. Maultzsch, F. J. Tegude and M. Schleberger, *J. Appl. Phys.*, 2013, **113**, 214306.

48 R. Chen, Q. Liu, J. Liu, X. Zhao, J. Liu, L. He, J. Wang, W. Li, X. Xiao and C. Jiang, *2D Mater.*, 2019, **6**, 034002.

49 J. Jadwiszczak, D. Keane, P. Maguire, C. P. Cullen, Y. Zhou, H. Song, C. Downing, D. Fox, N. McEvoy, R. Zhu, J. Xu,



G. S. Duesberg, Z.-M. Liao, J. J. Boland and H. Zhang, *ACS Nano*, 2019, **13**, 14262–14273.

50 J. Jadwiszczak, P. Maguire, C. P. Cullen, G. S. Duesberg and H. Zhang, *Beilstein J. Nanotechnol.*, 2020, **11**, 1329–1335.

51 C. Lee, H. Yan, L. E. Brus, T. F. Heinz, J. Hone and S. Ryu, *ACS Nano*, 2010, **4**, 2695–2700.

52 C. Kim, I. Moon, D. Lee, M. S. Choi, F. Ahmed, S. Nam, Y. Cho, H.-J. Shin, S. Park and W. J. Yoo, *ACS Nano*, 2017, **11**, 1588–1596.

53 Y. Jung, M. S. Choi, A. Nipane, A. Borah, B. Kim, A. Zangiabadi, T. Taniguchi, K. Watanabe, W. J. Yoo, J. Hone and J. T. Teherani, *Nat. Electron.*, 2019, **2**, 187–194.

54 Y. Guo, D. Liu and J. Robertson, *ACS Appl. Mater. Interfaces*, 2015, **7**, 25709–25715.

55 C. M. Smyth, R. Addou, S. McDonnell, C. L. Hinkle and R. M. Wallace, *J. Phys. Chem. C*, 2016, **120**, 14719–14729.

56 W. A. Saidi, *J. Chem. Phys.*, 2014, **141**, 094707.

57 A. Di Bartolomeo, A. Grillo, F. Urban, L. Iemmo, F. Giubileo, G. Luongo, G. Amato, L. Croin, L. Sun, S.-J. Liang and L. K. Ang, *Adv. Funct. Mater.*, 2018, **28**, 1800657.

58 H. Qiu, T. Xu, Z. Wang, W. Ren, H. Nan, Z. Ni, Q. Chen, S. Yuan, F. Miao, F. Song, G. Long, Y. Shi, L. Sun, J. Wang and X. Wang, *Nat. Commun.*, 2013, **4**, 2642.

59 J. Suh, T.-E. Park, D.-Y. Lin, D. Fu, J. Park, H. J. Jung, Y. Chen, C. Ko, C. Jang, Y. Sun, R. Sinclair, J. Chang, S. Tongay and J. Wu, *Nano Lett.*, 2014, **14**, 6976–6982.

60 S. Tongay, J. Suh, C. Ataca, W. Fan, A. Luce, J. S. Kang, J. Liu, C. Ko, R. Raghunathanan, J. Zhou, F. Ogletree, J. Li, J. C. Grossman and J. Wu, *Sci. Rep.*, 2013, **3**, 2657.

61 S. McDonnell, R. Addou, C. Buie, R. M. Wallace and C. L. Hinkle, *ACS Nano*, 2014, **8**, 2880–2888.

62 Y. Liu, J. Guo, E. Zhu, L. Liao, S.-J. Lee, M. Ding, I. Shakir, V. Gambin, Y. Huang and X. Duan, *Nature*, 2018, **557**, 696–700.

63 A. Pelella, O. Kharsah, A. Grillo, F. Urban, M. Passacantando, F. Giubileo, L. Iemmo, S. Sleziona, E. Pollmann, L. Madaufl, M. Schleberger and A. Di Bartolomeo, *ACS Appl. Mater. Interfaces*, 2020, **12**, 40532–40540.

64 K. Shahzad, K. Jia, C. Zhao, D. Wang, M. Usman and J. Luo, *Materials*, 2019, **12**, 3928.

65 T. Knobloch, G. Rzepa, Y. Y. Illarionov, M. Waltl, F. Schanovsky, B. Stampfer, M. M. Furchi, T. Mueller and T. Grasser, *IEEE J. Electron Devices Soc.*, 2018, **6**, 972–978.

66 H. Nan, Z. Wang, W. Wang, Z. Liang, Y. Lu, Q. Chen, D. He, P. Tan, F. Miao, X. Wang, J. Wang and Z. Ni, *ACS Nano*, 2014, **8**, 5738–5745.

67 S. Tongay, J. Zhou, C. Ataca, J. Liu, J. S. Kang, T. S. Matthews, L. You, J. Li, J. C. Grossman and J. Wu, *Nano Lett.*, 2013, **13**, 2831–2836.

68 S. Wang, X. Zeng, Y. Zhou, J. Lu, Y. Hu, W. Wang, J. Wang, Y. Xiao, X. Wang, D. Chen, T. Xu, M. Zhang and X. Bao, *ACS Appl. Electron. Mater.*, 2022, **4**, 955–963.

69 X. Wei, Z. Yu, F. Hu, Y. Cheng, L. Yu, X. Wang, M. Xiao, J. Wang, X. Wang and Y. Shi, *AIP Adv.*, 2014, **4**, 123004.

70 L. Kong, A. Enders, T. S. Rahman and P. A. Dowben, *J. Phys.: Condens. Matter*, 2014, **26**, 443001.

71 S. KC, R. C. Longo, R. M. Wallace and K. Cho, *J. Appl. Phys.*, 2015, **117**, 135301.

72 R. Degraeve, M. Cho, B. Govoreanu, B. Kaczer, M. B. Zahid, J. van Houdt, M. Jurczak and G. Groeseneken, *IEEE International Electron Devices Meeting*, 2008, Piscataway, NJ, 2008, pp. 1–4.

73 Y. Y. Illarionov, T. Knobloch, M. Waltl, G. Rzepa, A. Pospischil, D. K. Polyushkin, M. M. Furchi, T. Mueller and T. Grasser, *2D Mater.*, 2017, **4**, 025108.

74 D. S. Fox, Y. Zhou, P. Maguire, A. O'Neill, C. Ó'Coileáin, R. Gatensby, A. M. Glushenkov, T. Tao, G. S. Duesberg, I. V. Shvets, M. Abid, M. Abid, H.-C. Wu, Y. Chen, J. N. Coleman, J. F. Donegan and H. Zhang, *Nano Lett.*, 2015, **15**, 5307–5313.

75 K. Huang, M. Zhao, B. Sun, X. Liu, J. Liu, H. Chang, Y. Zeng and H. Liu, *ACS Appl. Electron. Mater.*, 2020, **2**, 971–979.

76 J. S. Kim, J. Kim, J. Zhao, S. Kim, J. H. Lee, Y. Jin, H. Choi, B. H. Moon, J. J. Bae, Y. H. Lee and S. C. Lim, *ACS Nano*, 2016, **10**, 7500–7506.

77 S. Ghatak, A. N. Pal and A. Ghosh, *ACS Nano*, 2011, **5**, 7707–7712.

78 K. S. Novoselov, D. Jiang, F. Schedin, T. J. Booth, V. V. Khotkevich, S. V. Morozov and A. K. Geim, *Proc. Natl. Acad. Sci. U. S. A.*, 2005, **102**, 10451–10453.

79 M. Amani, M. L. Chin, A. G. Birdwell, T. P. O'Regan, S. Najmaei, Z. Liu, P. M. Ajayan, J. Lou and M. Dubey, *Appl. Phys. Lett.*, 2013, **102**, 193107.

80 B. Chakraborty, A. Bera, D. V. S. Muthu, S. Bhowmick, U. V. Waghmare and A. K. Sood, *Phys. Rev. B: Condens. Matter Mater. Phys.*, 2012, **85**, 161403.

81 E. Pollmann, L. Madaufl, S. Schumacher, U. Kumar, F. Heuvel, C. vom Ende, S. Yilmaz, S. Güngörümüs and M. Schleberger, *Nanotechnology*, 2020, **31**, 505604.

82 Y. Guo, X. Wei, J. Shu, B. Liu, J. Yin, C. Guan, Y. Han, S. Gao and Q. Chen, *Appl. Phys. Lett.*, 2015, **106**, 103109.

83 K. Choi, S. R. A. Raza, H. S. Lee, P. J. Jeon, A. Pezeshki, S.-W. Min, J. S. Kim, W. Yoon, S.-Y. Ju, K. Lee and S. Im, *Nanoscale*, 2015, **7**, 5617–5623.

84 Y. Y. Illarionov, G. Rzepa, M. Waltl, T. Knobloch, A. Grill, M. M. Furchi, T. Mueller and T. Grasser, *2D Materials*, 2016, **3**, 035004.

85 E. Zhang, W. Wang, C. Zhang, Y. Jin, G. Zhu, Q. Sun, D. W. Zhang, P. Zhou and F. Xiu, *ACS Nano*, 2015, **9**, 612–619.

86 X. Hou, X. Yan, C. Liu, S. Ding, D. W. Zhang and P. Zhou, *Semicond. Sci. Technol.*, 2018, **33**, 034001.

87 T. Nagumo, K. Takeuchi, T. Hase and Y. Hayashi, *2010 International Electron Devices Meeting*, 06.12.2010–08.12.2010, 2010, pp. 28.3.1–28.3.4.

88 Y. G. Lee, C. G. Kang, U. J. Jung, J. J. Kim, H. J. Hwang, H.-J. Chung, S. Seo, R. Choi and B. H. Lee, *Appl. Phys. Lett.*, 2011, **98**, 183508.

89 A. Kumar, L. Viscardi, E. Faella, F. Giubileo, K. Intonti, A. Pelella, S. Sleziona, O. Kharsah, M. Schleberger and A. Di Bartolomeo, *J. Mater. Sci.*, 2023, **58**, 2689–2699.

90 G. Zschornack, M. Kreller, V. P. Ovsyannikov, F. Grossman, U. Kentsch, M. Schmidt, F. Ullmann and R. Heller, *Rev. Sci. Instrum.*, 2008, **79**, 02A703.

